Electronic structure, Schottky barrier, and optical spectra of the SiC/TiC {111} interface

Sergey N. Rashkeev,* Walter R. L. Lambrecht, and Benjamin Segall
Department of Physics, Case Western Reserve University, Cleveland, Ohio 44106-7079
(Received 3 January 1997)

A first-principles total energy and electronic structure study of 3*C*-SiC/TiC {111} interfaces was carried out using the full-potential linear-muffin-tin orbital method. Three distinct plausible structural models were identified and investigated including the relaxation of the most important structural degrees of freedom. All three models considered have a threefold symmetry axis and have a mutual boundary layer of carbon. They were found to be stable with respect to small rigid body translations parallel to the interface which would destroy the threefold symmetry. One of the models (*B*) is a twinned version of the other (*A*) while the third model (*C*) differs from *A* by a rigid body translation parallel to the interface. The *A* and *C* models contain a common carbon sublattice in both the zinc blende structure of the SiC and rocksalt structure of the TiC. While in model *A* the Ti's are on top of the Si atoms nearest to interface, they are in a hollow site between the Si atoms in both the *B* and *C* models. Model *A* is found to be metastable with a significantly higher energy than *B* and *C*. This is explained in terms of the occurrence of compressed Ti-Si nearest neighbor distances in the ideal structure. The expansion of the latter disrupts the interfacial Ti-C bonding. Our calculations find very nearly equal energies for the relaxed *B* and *C* models. This indicates that the occurrence of twinned (untwinned) structures on flat (stepped) surfaces as has been observed by electron microscopy is probably not due to a thermodynamic preference but rather to kinetic factors such as step-flow growth. All three structures have interface states in the band gap of SiC which are localized within two lattice planes from the interface and which pin the Fermi level. The nonbonding character of these interface states leads to nearly equal Schottky barriers for all three models. The optical dielectric functions for our interface models were calculated and show signatures of these interface states which should be detectable in the infrared range because of their strong anisotropy with respect to the interface plane. [S0163-1829(97)00124-0]

I. INTRODUCTION

Recently, great progress has been made in developing silicon carbide (SiC) for high-temperature, high-speed, and high-power device applications.[1] However, an important technological problem presently limiting device performance in some instances is the fabrication of high-temperature stable, low-contact resistance Ohmic contacts. It would also be desirable to be able to fabricate high ideality Schottky barrier metal contacts on SiC. The presently widely followed approach for achieving Ohmic contacts is to heavily dope the semiconductor and to use annealing treatments to create a gradual transition layer. The Ohmic behavior in such a case results from tunneling through the barrier, but the actual band line up is Schottky-like. This tunneling behavior usually results in an undesirably high specific contact resistance unless the barrier is quite thin. Defect free, sharp epitaxial interfaces are desirable to reduce the contact resistance of Ohmic contacts as well as to increase the ideality factor of Schottky barriers.[2] An ideal zero resistance Ohmic contact is one with a zero Schottky barrier. We define the *p*-type Schottky barrier height (SBH) as the Fermi level of the metal E_F minus the valence band maximum E_v of the semiconductor, i.e., $\Phi_B^p = E_F - E_v$ and likewise the *n*-type Schottky barrier as $\Phi_B^n = E_c - E_F$, where E_c is the conduction-band minimum. One thus needs to find metals or metal compounds and/or surface modifications that allow one to control Φ_B^p from zero (for *p*-type contacts) to the band gap (for *n*-type contacts). To this end a better understanding of the Schottky barrier formation is a prerequisite.

Several metal depositions on SiC have been studied. A recent review was compiled by Kaplan and Bermudez.[3] Most metals lead to Schottky behavior in the as-deposited state. Upon heat treatments, however, most pure metal deposits, in particular transition metals, are not stable but participate in chemical reactions. The situation is not unlike that of metals on silicon although the complexity is far greater because both silicides and carbides can form. Because these compounds are typically metallic, the metal-semiconducting interface is actually displaced to the silicide-SiC or carbide-SiC interface.

Among the various metals studied, Ti is of particular interest. Although it can form silicides as well as carbides, TiC has been shown to form as first phase next to the interface,[4–8] and/or as isolated particles near the interface. As carbon from the SiC is consumed in the reaction with Ti to form the rather stable TiC, a more and more Si-rich environment results for the Ti farther away from the interface. This Si can diffuse through the TiC and subsequently form Ti silicides such as Ti_5Si_3 and $TiSi_2$. These results from solid-reaction studies are consistent with an Auger and low energy electron diffraction study by Bellina and Zeller.[9] They found that thin Ti deposits on SiC first ''attack'' the surface carbon layers if the starting surface conditions are carbon-rich and subsequently start to break up the SiC with the excess Si segregating to the surface. Recently, Parsons *et al.*[10–12] have shown that this problem, the deterioration of the semiconductor, can be overcome if TiC itself is deposited in stoichiometric conditions by chemical vapor deposition. It was then

found to be in stable coexistence with SiC without formation of Ti silicides up to at least 1400 °C. They reported thermally stable Ohmic contacts with specific contact resistances below $6\times10^{-6}\ \Omega\ \mathrm{cm}^2$ on *n*-type 3*C*-SiC (Ref. 10) and of an order of $1.3\times10^{-5}\ \Omega\ \mathrm{cm}^2$ on *n*-type 6*H*-SiC.[11]

TiC has several potential advantages as a contact metal: (1) it is a hard and high-temperature resistant (i.e., refractory) metallic compound, (2) it is closely lattice matched to SiC, and (3) there exist a class of related transition metal and rare-earth carbides and nitrides with closely related properties and identical crystal structure, offering the potential for tuning the properties of the interface by making suitable solid solutions. For example, TiN and TaN have been suggested[9] as effective diffusion barriers to limit the reaction which would otherwise continue to consume the carbon from the SiC substrate. TiN, having a somewhat lower work function (3.75 eV) than TiC (4.0–4.4 eV),[13] was thus suggested by Glass *et al.*[14] to be a good candidate for Ohmic contacts. Ohmic behavior was indeed found as deposited but with a rather high-contact resistance of order $10^{-2}\ \Omega\ \mathrm{cm}^2$.

It is of interest to note that TiC, which has the cubic rocksalt structure, has also been used rather successfully[15–19] as a substrate for epitaxial growth of 3*C*-SiC because the lattice mismatch is only 0.6% and it was hoped that a cubic substrate would facilitate the stabilization of cubic SiC. Considerable effort has been spent growing large monocrystalline TiC boules with low defect densities for this purpose.[18] While this approach has recently been essentially abandoned in favor of bulk 6*H*-SiC and 4*H*-SiC substrates which result in better epitaxial film quality, these efforts have shown that epitaxial interfaces of TiC and SiC are possible. Transmission electron microscopy (TEM) and high resolution electron microscopy (HREM) investigations have shown that the resulting interfaces between TiC and SiC can be atomically flat.[19] HREM imaging of as-deposited Ti/6*H*-SiC interfaces and of 6*H*-SiC/TiC/Ti_5Si_3 interfaces obtained after annealing has also been achieved.[5] The possibility of growing TiC on SiC and vice versa is also of interest because it opens possible new avenues for device fabrication such as metal base transistors and metal layer resonant tunneling devices. The feasibility of the latter has recently been demonstrated for the ErAs/GaAs system[20–22] which has the same crystallographic relationship between its components as TiC/SiC.

The TEM studies of Chien *et al.*[19] provide rather detailed information on the structure of the SiC/TiC interfaces because high-resolution imaging was possible. They show that {001} interfaces are generally rough with only small regions of atomically sharp interfaces. The {111} interface on the other hand was found to exhibit large regions of atomically sharp interfaces. Furthermore, two distinct configurations were identified. In both cases, the main crystallographic directions of the cubic rocksalt and zinc blende structures are parallel and there appears to be a common carbon sublattice. However, on large flat terraces, the {111} family of planes [besides the interface (111) plane] are twinned with respect to the substrate while on small terraces, they were untwinned. The small terraces occurred by (111) faceting of the (112) plane. From that paper, it is not clear if this faceting occurred as a result of the SiC growth or was present beforehand on the surface of TiC. Tentative atomic structures for these interfaces were proposed based on HREM image simulations. Bow[6] also found a similar interface orientation for TiC formed by Ti reactions on 6*H*-SiC. The TiC {111} planes were found to be twinned with respect to the last three (cubically) stacked layers of the 6*H*-SiC. These observations raise questions about the relative energy difference of the twinned and untwinned interface configurations as well as their differences in electronic properties. The band lineup, i.e., SBH of these interfaces has not yet been conclusively determined. Porter *et al.*[7] reported *I-V*, *C-V*, and x-ray photoelectron spectroscopy (XPS) measurements of the barrier heights of as-deposited and annealed Ti/SiC interfaces, but the inhomogeneity of the interfaces resulting from the annealing did not allow them to associate this exclusively with TiC/SiC.

In view of the detailed structural information available for this system and its potential technological promise, the SiC/TiC system can be considered an interesting prototype system for SiC/metal contacts worth further investigation. The lattice match also facilitates its theoretical study. Determining the optimum interface structure between a rocksalt and a zinc blende structure is of intrinsic interest because of the frustration of the directed bonding types at the interface: octahedral in rocksalt and tetrahedral in zinc blende. Because this problem is expected to have some intrinsically geometric aspects, a study of the TiC/SiC interface may also provide insights for other related interfaces, such as TiN/SiC. As already mentioned, a large family of potentially useful metallic compounds share the rocksalt structure with TiC and most semiconductors have the zinc blende structure.

The {001} SiC/TiC interfaces were investigated earlier by Lambrecht and Segall.[23] Although a rather complete set of structural models was investigated, the use of ideal bulk terminated structures and the atomic-sphere-approximation (ASA) muffin-tin orbital method in that work did not allow the authors to conclusively determine the interface structure. It was found that most configurations gave rise to unfavorable bond distances and consequently had rather high energy. One exception was a model with Ti directly on top of Si atoms of Si terminated SiC. It could not be excluded, however, that other models would obtain lower energy by relaxation. As a general feature, because the {001} surface of TiC contains both Ti and C, an adjustment of both types of bond lengths would require buckling of the terminating TiC plane. This would then also affect bond distances to the next layers. Hence, one might expect the relaxation to be several layers deep. Since there are several models to consider, the problem would be rather formidable without guidance from experiment. As already mentioned, the {001} interfaces are usually found to be rough. This may indicate that several competing low energy configurations exist and conflict with each other as a result of independent nucleation events.

Fortunately, the situation for the {111} interface is somewhat simpler, and, therefore chosen as the subject of the present investigation. Since {111} planes of TiC and SiC contain only one type of atom, one may expect that the important relaxations involve only adjustments of interplanar spacings limited to the layers immediately adjacent to the interface. Finally, the {111} plane of SiC is structurally similar to the {0001} plane of the hexagonal and rhombohedral polytypes of SiC (e.g., 4*H*, 6*H*, 15*R*, collectively denoted as α-SiC). The results for the interface structure of TiC on the

{111} plane 3C-SiC are thus expected to be relevant for those on {0001} planes of α-SiC.

In this work, we thus focus on the {111} SiC/TiC interface. Full potential linear-muffin-tin orbital calculations were carried out for three models, which were suggested by the HREM investigation. Structural relaxations are included. These allow us to address the question of the relative stability of the models. In fact, we find a low energy model for both the twinned and untwinned interfaces mentioned above and find them to have locally similar bonding configurations for the interface Ti atoms. In the untwinned case, however, this model requires a rigid body translation parallel to the interface. This and the other implications for the structure are discussed in connection with the available HREM information. A third, significantly higher energy, metastable interface configuration for the untwinned case is also found and discussed.

Schottky barrier heights and details of the electronic structure were obtained from the calculations. They show that Fermi level pinning by interface states determines the Schottky barrier height, a conclusion which was also reached in the previous work on SiC/TiC {001}.[23]

We find that the Schottky barrier height is almost the same for the various models investigated, including the higher energy metastable state. This seemingly surprising result is subsequently explained in terms of the nature of the interface states pinning the Fermi level. Since experimental verification of this is important we also investigate whether these interface states could possibly be detected by optical spectroscopies. To this end, we calculate the optical response functions of our model systems.

The paper is organized as follows. In Sec. II we provide the necessary details on the computational method. In Sec. III we describe the supercell models used to study the {111} SiC/TiC interface. This is not entirely trivial because we need to find ways to make the proposed interface structural models compatible with three dimensional (3D) periodicity required for the band-structure calculations. We also describe the interface degrees of freedom that were relaxed. The results section, Sec IV, is divided as follows: Sec. IV A provides our total energy results for the various structures and a discussion of the relaxation and bonding; Sec. IV B contains the results for the Schottky barrier heights; Sec. IV C presents the electronic structure of the models in terms of local densities of states and state charge density plots and discusses their role in establishing the Schottky barrier height and the relative stability of the models. In Sec. IV D we present our theoretical calculations of the optical spectra. Section V contains a summary of our main conclusions. Some preliminary results of the present study were previously published in a conference proceedings.[24]

II. METHODS

The calculations of the total energy and electronic structure were carried out within the framework of density functional theory in the local density approximation (LDA) using the exchange-correlation parametrization of Hedin and Lundqvist.[25] We employed the full-potential linear-muffin-tin orbital (FP-LMTO) method introduced by Methfessel.[26] This allows one to treat potentials of general form both within nonoverlapping muffin-tin spheres and the interstitial region. Before embarking on the time-consuming relaxation studies, we performed some convergence studies to reduce the basis set to a minimal one while maintaining sufficiently accurate total energies and band structures. Double κ basis sets, specifically dp for Si (meaning up to $l=2$ for the first [$\kappa^2=-0.01$ Ry] and up to $l=1$ for the second [$\kappa^2=-1$ Ry]), dd for Ti and pp for C were employed in the final calculations. Here, $\kappa^2=E-v_{\mathrm{mtz}}$ is the difference between the energy of the spherical wave and the muffin-tin zero. It determines the decay length of the Hankel envelope functions of the muffin-tin orbitals. Also, we included a second panel which contains the pseudocore 3p states of Ti. These states are important for the convergence of the self-consistent procedure as observed in calculations of TiC, TiN, and TiO.[27]

As usual for the relatively open structures encountered here, two empty spheres per unit cell of both the zinc blende and rocksalt structures were used for the augmentation of the muffin-tin orbitals. No basis sets centered on these sites were used, however, so as to keep the basis set minimal. The augmentations and auxiliary fitting Hankel functions were expanded to $l_{\max}=4$. The radii of all spheres were kept the same in the bulk parts of the cells. For the untwinned model (model A below), we found that this was possible with reasonably large radii even at the interfacial layers in the presence of relaxation. It is possible for this case because the unrelaxed lattice (body-centered cubic) of all sites, including those for the empty spheres, is uniform throughout the whole structure. This situation does not prevail for the twinned model. In that case, the space available for an empty sphere near the interfacial carbon atoms and the neighboring Ti atom is small. Instead of using a small sphere there, we have found it preferable to just eliminate that sphere. The error introduced thereby is found to be small, specifically, much smaller than the energies characterizing the relaxation processes. The interface empty spheres in the untwinned A model, see below, were scaled with the increasing distance in this region in the course of the relaxation.

A symmetry reduction of the number of k points was effective using the sampling procedure of Methfessel and Paxton.[28] The number of irreducible k points varied from 20 for the calculations of the self-consistent electronic density to 230 for the densities of states.

The particulars of our calculation of Schottky barrier heights and of the optical response functions of the interfaces are given along with the corresponding results in later sections.

III. STRUCTURAL MODELS

As noted in the Introduction we will be concerned with the {111} interface of rocksalt TiC and zinc blende SiC. The {111} planes of both of these are polar planes, indicating that they contain only one type of atom. In principle, there are thus four possible terminations to consider: Si or C for the SiC and Ti or C for the TiC. Since the bonding has a partially ionic character in both materials with Ti and Si playing the role of cations and C the role of anion, it is unlikely to lead to Ti-Si or C-C as pairs of interface planes. We thus expect a mutual boundary layer of C atoms which can then

be considered to be the terminating plane of both the TiC and SiC. This assertion may seem to be at odds with the previous result[23] which found Ti on top of Si to be a low energy configuration for the {001} interface. However, the {001} TiC plane is neutral as it contains both Ti and C ions. In addition, that arrangement was found to result mainly from a more favorable Ti-Si separation in the low-energy configuration than in the other unrelaxed geometries. We will show below that the Ti-Si distance also plays a crucial role for the {111} interfaces.

Further information allowing us to limit our search for plausible low energy structures comes from experiment. The HREM and selected area diffraction studies by Chien *et al.*[19] show that the crystallographic directions of the two crystal lattices are parallel, except for a stacking alternation leading to twinning at the interface in one of the two interface configurations that were observed. The HREM images show essentially a continuation of the lattice planes. However, this must be viewed with some caution because it is not *a priori* clear whether the bright spots in the HREM images correspond to atoms or to voids. Also, since we see only one cross section, lateral displacements perpendicular to the image plane cannot be excluded. Nevertheless, the images suggest a simple structure which can be described as follows: the zinc blende and rocksalt structures— both of which consist of two interpenetrating fcc lattices— share a common fcc sublattice of carbon atoms in the bicrystal. A common fcc sublattice of anions was also conclusively proven by ion channeling studies for the case of ErAs/GaAs, another example of a rocksalt/zinc blende interface.[29]

Having decided that SiC should end in a C layer, we still have two possibilities: either the second layer Si atoms lie directly beneath the C atoms which then results in three dangling bonds sticking out into the interface region, or, they sit in the centers of the triangular array of C atoms, in which case there is only one dangling bond. Since the latter is energetically more favorable for a free surface, it is reasonable to take it to be the preferred starting point for the interface formed by TiC growing on SiC. In the experiments of Chien *et al.*,[19] however, SiC was grown on the TiC. Nevertheless, one may still argue that the number of SiC terminating C-dangling bonds at the interface should be minimized in a low energy configuration.

The above considerations lead immediately to the two models *A* and *B* shown in Fig. 1 for the untwinned and twinned configurations of the carbon planes, respectively. In model *A* the carbon atoms can indeed be seen to form a continuous sublattice throughout the structure, while in model *B* the TiC part of the sublattice has been rotated by 180° about a {111} direction thus forming a coherent {111} twin boundary at the interface plane. We note that both models contain a threefold symmetry axis. In general one would expect that high symmetry configurations are more likely to correspond to either local maxima or minima in the total energy. We thus restrict our attention initially to configurations maintaining a threefold symmetry axis at the interfaces.

From a local bonding point of view, the main difference in the models is that in *A* the interfacial Ti sits directly above the interfacial Si layer while in *B* it sits in the center of the triangle of the Si atoms. In both models, the common carbon layer sits in the correct position to form bonds with either Ti or Si because it is a continuation of each of the two crystal lattices.

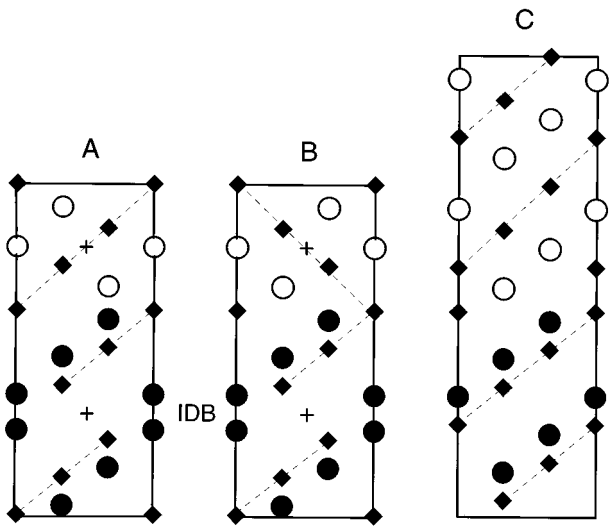

FIG. 1. Structure of the *A*, *B*, and *C* models of the SiC/TiC {111} interface. Models *A* and *B* are shown in the IDB geometry, while a 6+6 layer slab+slab geometry is used for model *C*. The carbon (diamonds), silicon (black circles), and titanium (white circles) atoms displayed are all in one plane. The crosses indicate centers of inversion, and the dashed lines emphasize that the carbon planes are parallel in the TiC and SiC components of *A* and *C* while they are twinned in *B*.

Next, we consider the main degrees of freedom for the interface atoms which should be relaxed, while retaining the essential aspects of these structural models. We should distinguish here between rigid body displacements and individual atomic displacements. In a rigid body displacement, i.e., a translation of the whole TiC half crystal with respect to the SiC half crystal, the bonding within each unit remains perfect, only the interfacial bonding is affected. Clearly, this is energetically preferable to moving the interface atoms separately while keeping the bulk layers fixed because that would disrupt the bonding of the interface layers to the bulk-like layers. The simplest type of rigid body displacements are those perpendicular to the interface. Since the carbon layer in some sense belongs to both half crystals, we allow both the nearest neighbor Ti and Si layers to it to be displaced independently, with rigid shifts of the attached TiC and SiC half crystals.

The initial calculations of the models indicated that model *A* is unfavorable compared to *B* because the Ti sits directly above the Si. Subsequently it was shown that the forces resulting from small lateral displacement on the interface atoms vanished. This confirmed that these configurations are local minima. There is, however, another configuration closely related to the untwinned case which also has a threefold axis.

Considering the close-packed triangular lattice of carbon atoms in the interface layer, there are three sets of threefold symmetry axes: the ones through the atoms and the ones through the centers of the triangles pointing upwards or downwards (the so-called *A*, *B*, or *C* positions, in the usual nomenclature, which are not to be confused with the present labels for the interface configurations.) Thus, a rigid body

translation parallel to the interface which maintains threefold symmetry is possible. In particular, a shift which brings the interfacial Ti atoms in the same position with respect to the underlying SiC as in model *B* seems a plausible candidate for a low energy structure. We label this model *C* and further relax it with respect to rigid body displacements perpendicular to the interface. As will be discussed below, that structure was found to have a lower energy than that for *A* and very close to that for *B*.

The next step is to make these interface models compatible with 3D periodicity so as to enable us to use band-structure methods for calculating the total energy. The most commonly used procedure is to repeat the interfaces periodically. This, however, automatically introduces a second interface. In structures of sufficiently high symmetry, the two interfaces can be chosen to be equivalent. However, because the {111} surface of the zinc blende structure is not a mirror plane and the lattice has no inversion center, it is impossible to obtain a periodic supercell with two equivalent interfaces. Only special techniques focusing on local energy contributions allow one to extract individual interface energies in such cases.[30,31] We have taken two different approaches to handle this problem.

In the first one, we introduce inversion domain boundaries (IDB's) in the middle of the SiC part of the cell. This approach was followed for our study of models *A* and *B*, but not for *C* for the reasons given below. It was previously used in calculations of GaAs {111} surfaces by Kaxiras *et al.*[32] Since as discussed above the SiC part is terminated in a carbon layer with a single dangling bond, the other end of each SiC half ends in a Si layer with a single dangling bond. The IDB's thus consist of Si-Si bonds. The specific model unit cells used in our calculations consist of six SiC double layers and a five atomic layer TiC unit (Ti-C-Ti-C-Ti) as depicted in Fig. 1. We will refer to such arrangements as the IDB geometry. We will show that the IDB does not have a significant effect on any of the results for the layers adjacent to the SiC/TiC interface.

These supercells involve about 30 atoms (including empty spheres), a number which is sufficiently small to allow us to conveniently carry out total energy calculations including atomic relaxations. We also note that these cells have two centers of inversion. Since the IDB stays the same in the two models in which it is used, we can meaningfully compute the relaxation of each of the interface models and compare their interface energies. If the IDB energy were known separately, which could be done following the approach of Ref. 30, we could obtain the absolute interface energies from

$$[2\gamma_i+\gamma_{\mathrm{IDB}}]S=E_{\mathrm{supercell}}-E_{\mathrm{bulk\ TiC}}-E_{\mathrm{bulk\ SiC}}-\sum_{\alpha}N_{\alpha}\mu_{\alpha}, \tag{1}$$

where γ_i and γ_{IDB} are the interface and IDB energies per unit area, S is the unit cell area, $E_{\mathrm{supercell}}$ the total energy of the supercell, $E_{\mathrm{bulk\ TiC}}$ and $E_{\mathrm{bulk\ SiC}}$ the total energies of corresponding numbers of TiC and SiC layers in the bulk, and N_α is the excess number of atoms of species α per unit cell and μ_α their chemical potential. The last term allows one, for example, to introduce extra Ti atoms in the cell to produce a cell of a convenient shape and size. It requires one to specify the range of possible values of the chemical potential. For example, for excess Ti atoms, we would have

$$\mu_{\mathrm{Ti}}^0>\mu_{\mathrm{Ti}}>\mu_{\mathrm{Ti}}^0+\Delta H_f(\mathrm{TiC}), \tag{2}$$

where μ_{Ti}^0 is the energy of a Ti atom in bulk Ti, and ΔH_f(TiC) is the energy of formation of TiC out of bulk Ti and bulk (say graphite) C. We have not carried out the separate calculations of the IDB energy or of the separate Ti and C energies here because there is no need at this point to know the absolute value of the interface energy. Since models *A* and *B* have exactly the same number of Ti and C atoms and SiC units and the IDB energy is essentially the same in both, all of the corresponding terms drop out of the difference of the energies for *A* and *B*. We find

$$2S(\gamma_i^A-\gamma_i^B)=E_{\mathrm{supercell}}^A-E_{\mathrm{supercell}}^B. \tag{3}$$

The above-mentioned terms also drop out of the relaxation energy for each of the models separately.

Unfortunately, comparable IDB cells for the *C* model introduce problems. A supercell of the same size as that used for *A* and *B* involves a different geometry: its translation vector lying out of the interfacial plane is not orthogonal to that plane. The mesh of the *k* points generated in such a case will be different from that for the *A* and *B* cells. That is undesirable for an accurate comparison of the total energies. On the other hand, one can construct an orthogonal cell with two equivalent interfaces, but in that case we need four layers of Ti and three of C instead of three and two as in models *A* and *B*. While this is not an essential problem since the extra energy of a bulk TiC layer can easily be subtracted out, it is nevertheless preferable to have equal size supercells with the same geometry when calculating energy differences. This ensures that all relevant energies are converged in exactly the same manner and it minimizes the effects of systematic errors. We thus used an alternative approach. That has the added advantage that when applied to the *A* and *B* models it provides a check on the results obtained from the IDB geometry. In this approach, we choose supercells which have a double-slab geometry. Specifically they contain three units of TiC and three double layers of SiC (or six units of TiC and six layers of SiC) again with a mutual carbon layer at the interface. At the other ends of the cell, the SiC and TiC are separated by a ''vacuum'' which we take to be two layers of empty spheres. Such arrangements will be referred to as the ''slab+slab geometry.'' This approach introduces two additional interfaces, namely, a ''SiC-vacuum'' and a ''TiC-vacuum'' interface. Both of these involve dangling bonds which are expected to contribute states near the Fermi level. However, we will show below that the effects of these states on observables of interest such as the Schottky barrier can easily be excluded. Although the real surfaces can be expected to exhibit relaxations, this need not concern us here since the surface energies of the present models again drop out of the relevant energy differences. In this approach, the energy associated with the translation involved in going from *A* to *C* can straightforwardly be evaluated by subtracting the supercell total energies without any need for additional calculations and without having to worry about equal convergence of bulk and supercell energies. A final advantage of

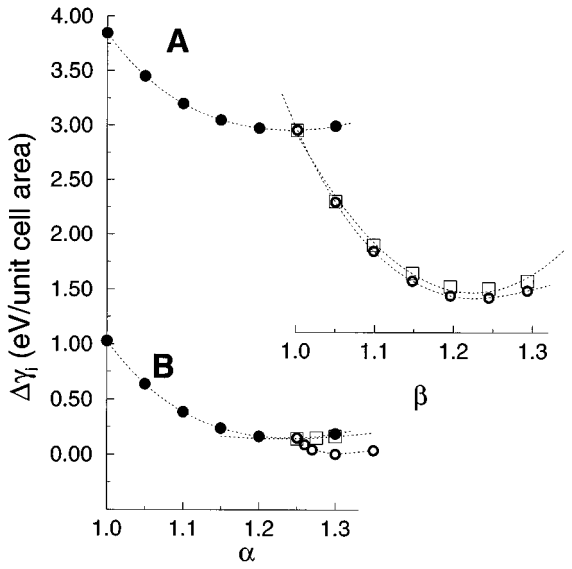

FIG. 2. Relaxation of the total energy of structures *A* and *B* in the space of two parameters α and β. α corresponds to IDB bond relaxation and is indicated with filled circles. β corresponds to SiC/TiC interface plane relaxation and is indicated with open circles when performed in the IDB geometry and with squares when done in the slab models. The β-relaxation results for the C structure (carried out only in the slab geometry) essentially overlap those for the *B* model and consequently were not included. The energy shown is normalized per interface unit cell area and given relative to the lowest energy of model *B*. Dotted lines indicate best fits through the calculated points and were used to obtain the energy minima.

the slab + slab geometry is that small lateral displacements away from the threefold symmetry can be taken into account.

IV. RESULTS

A. Structural relaxations

1. IDB geometry

Our first step in determining how the IDB affects the electronic structure at the interface, and, in particular, the total energy differences is to consider the relaxation of the distance *s* between the two Si layers in the IDB. The separation *s* is expressed as $s=\alpha s_0$, where s_0 is taken to be the pure SiC bond length (1.88 Å). The energies of the two structures as a function of α (while keeping the rest of the structure ideal) are shown in Fig. 2 as the filled circles. The energies displayed are relative to an arbitrary reference (whose choice will become clear later) and divided by a factor two. The reason for the halving is that then the energy differences give the change in interface energy between model *A* and *B* per interface unit cell area [see Eq. (3)]. It can be seen that the bonds in both structures relax to $\alpha=1.24$ or $s=2.25$ Å. For comparison, the bond in pure Si is 2.35 Å. Most significantly for our purpose, the curves for the *A* and *B* structures are virtually identical except that the curve for the energy of the twinned structure being rigidly displaced below that for the untwinned structure by the substantial amount of 2.8 eV/unit cell area. This provides evidence that the IDB behaves as an independent entity with a total energy difference contribution localized to its immediate vicinity. It will thus not appreciably influence our conclusions about the TiC/SiC interface.

Our next and more important concern involves the relaxation of the atomic positions in the interfacial layers in both structures. We first assume that all the interplane distances (Si-C, C-Ti, Si-Ti) in the interfacial region change homogeneously, i.e., are all expanded by the same factor β. Since the Ti and Si are cations in their respective sublattices we expect them to repel each other, i.e., for β to relax to a value greater than one. Subsequently, we checked that separate relaxations of the Si-C and C-Ti interplane distances gives practically the same result as the simplified homogeneous model. For simplicity we only show the results of the homogeneous model.

Figure 2 displays the energies for the two structures as a function of β by the open circles with the value of α fixed at the value 1.24 found above. It can be seen that the relaxation at the interface is much larger for, and has a much greater effect on, the higher energy *A* than lower energy *B* structure. The energy differences between the minima is reduced to about half the unrelaxed difference. Nevertheless, the twinned structure remains the distinctly lower energy structure.

The final calculated energy difference between relaxed models *A* and *B* is $\Delta\gamma_i=2.8$ J/m^2 or 1.43 eV/unit cell area (i.e., per Ti atom). The relaxation energies of model *A* and *B* are, respectively, -3.1 J/m^2 and -0.3 J/m^2.

2. Slab+slab geometry

As mentioned in Sec. III, by using the slab + slab geometry we were able to check the interface relaxations found for the IDB geometry, and, in addition, to study the structure *C* and the effects of small lateral displacements away from threefold symmetry. The relaxation in terms of the β scaling parameter was calculated in the same manner as in the IDB models. These results are shown in Fig. 2 by means of the open squares. We found the minimum for the *A* model at the same β value, 1.23, found above, and for the *B* model $\beta=0.98$, i.e., close to the ideal distance. The relaxation energies of -2.9 J/m^2 in the *A* case and almost zero in the *B* case are also in good agreement with the IDB results. For the interface energy difference we find $\Delta\gamma_i=3.2$ J/m^2. Although the precise values differ slightly from the IDB results, the conclusion is the same. This gives us confidence in the applicability of the slab + slab geometry thus allowing us to investigate structural modifications which would be difficult to address with the IDB model.

Next, we checked the stability of models *A* and *B* against lateral displacements away from the threefold symmetry. To calculate the change of the total energy due to such a transformation we made a rigid shift of the TiC part of the cell along the horizontal axis in Fig. 1 without moving the interfacial carbon layer. For shifts up to the order of 0.1–0.2 of the lattice constant, the total energy increased monotonically in both the structures *A* and *B* (which were initially relaxed). This provides a strong support for our previous assumption that the structures *A* and *B* with the threefold symmetry axis are stable with respect to small tangential shifts, i.e., they represent at least a local energy minimum.

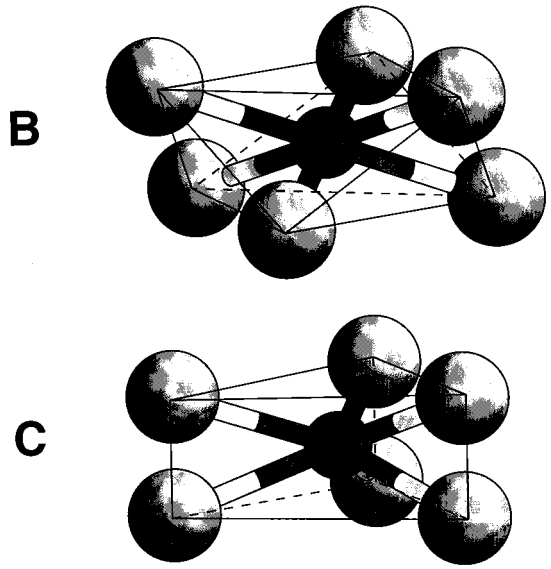

FIG. 3. Nearest neighbor carbon environments of the interfacial Ti atom in the *B* and *C* models.

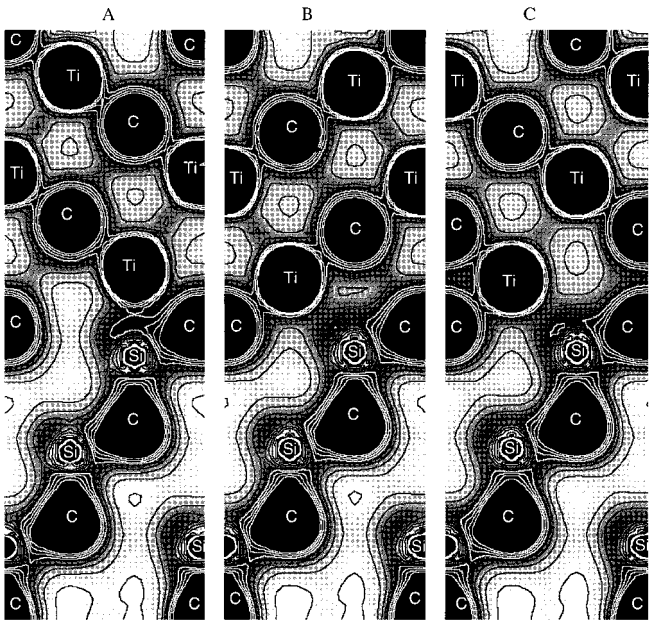

FIG. 4. Charge densities in models *A*, *B*, and *C* shown as a gray scale and contour lines calculated in 3+3 slab models. The plane passes through the nuclei of all atoms indicated and is the same as in Fig. 1.

Finally, we examine the *C* model. Its energy minimum is reached at the value of the parameter β close to unity and hence very close to that for the *B* structure. Since its dependence on β is also close to that for *B* its values were not included in Fig. 2. Moreover, the absolute value of the total energy for the *C* structure was found to be almost the same as for the *B* structure. It is actually found to be lower by 8 meV/atom. However, we consider this to be too small an energy difference to be significant. We thus conclude that to the precision of these calculations the *B* and *C* models are essentially degenerate in energy.

3. Local bonding environment analysis

The closeness in the energies and in the (β) relaxations for the *C* and *B* models, which have the same Ti position relative to the SiC surface, indicates that this relative positioning is the most important factor in determining the interface energy. In both the *C* and *B* structures, the Ti sits simultaneously above the centers of the triangles formed by nearest neighbor interface *C* atoms and above the second layer interface Si atoms. The difference between the two is that in the *B* model the carbon atoms in the next layer on the TiC side sit above the underlying Si atoms while in the *C* model it sits above the interface *C* layer. This is illustrated in Fig. 3.

The nearest neighbor cage of *C* atoms around the interface Ti is thus the usual octahedron in *B* while it is a triangular prism in *C*. While the *B* model thus provides a nearest neighbor cage exactly as in bulk TiC, and thus might be expected to have a significantly lower energy, this turns out not to be the case. The charge density plots in Fig. 4 show that the bonding of the interface Ti to the interface C is very similar to that to its *C* neighbor on the TiC side in both the *B* and *C* models.

In contrast, in the pure *A* position, the Ti sits directly above the second layer Si atoms. In the unrelaxed position the Ti-Si distance is 1.88 Å, whereas after relaxation it becomes 2.30 Å. Even so, it is still considerably smaller than a typical Ti-Si distance in Ti silicides which fall in the range $2.64 \leqslant d_{\text{Ti-Si}} \leqslant 2.80$ Å.[33] This suggests that the high energy of the *A* configuration is due to the repulsion between Ti and Si whose nearest neighbor distance is unfavorably compressed. In the *C* and *B* models on the other hand, the Ti sits at the more comfortable distance of 2.59 Å from the Si atom. The charge density plot, indicates that in models *B* and *C* there is rather little Ti-Si bond charge, suggesting little interaction at all between Ti and Si. This is because of the nature of the hybridization of the Ti orbitals which are already strongly participating in Ti-C bonds.

The reason why the Ti-Si distance in the *A* model cannot be stretched further can be understood as follows. Suppose that the interface carbon atoms stay fixed with respect to the underlying Si atoms so as to maintain their tetrahedral bonding environment as closely as possible. Then the bonding of the Ti to the interface carbon C_i weakens as the Ti recedes from the interface. On the other hand, if the C_i were to move along with the Ti, the Si-C_i bonding underneath would weaken. Our calculations indicate that the ratios of the Ti-C_i and Si-C_i to Ti-Si interplanar distances, with their sum equaling the Ti-Si distance, stay the same during the relaxation, meaning that some compromise between the two above tendencies occurs. In either case, we see that this weakening of the Ti-C_i and/or Si-C_i bonds will limit the extent to which the Ti-Si distance can be expanded.

The charge densities exhibited in Fig. 4 reveals that there is actually more charge in the Ti-Si bond region in the model *A* than in the other two. Furthermore, there is clearly a much weaker bonding of the Ti to the C_i in that model. This shows that the bond-length analysis alone given in the preceding paragraphs does not reveal the complete story. From the point of view of the charge densities, we see that models *B* and *C* are characterized by three strong interface Ti-C bonds

and three rather weak Ti-Si bonds. In model *A*, there is a somewhat stronger Ti-Si bond (which should nevertheless be weaker than in the Ti silicides because of the remaining bond compression); but there is only one of these and the three Ti-C interface bonds are significantly weaker than in the other structures. So from this point of view it is rather the weakened Ti-C bonds that are responsible for the higher energy of the *A* model. It is, however, interesting to note that this severing of the Ti-C_i bonds results from the repulsion between the Ti and Si.

One other point revealed in Fig. 4 is worth observing. In the *C* model, the C atoms in the second layer on the TiC side is sufficiently close to the interfacial C_i atoms that there is a nonnegligible interaction between the two. Effects manifested by this will be noted below.

Having rationalized the total energy differences in terms of bond-length relaxations and total charge densities and interplanar forces, it would at this point be desirable to further confirm these interpretations by inspection of the interface electronic densities of states. That is done below in Sec. IV C. Before that, however, we will compare our structural results with the HREM results.

4. Comparison to HREM

A rigid body translation like that in our *C* model was not discussed explicitly by Chien *et al.*[19] Nevertheless it is clear from the suggested crystal structures in their paper and from the electron micrographs that Ti atoms do not sit directly on top of Si atoms in the untwinned case. Thus those image most likely corresponds to our *C* model rather than to our *A* model. This inference is also consistent with the absence of a substantial interplanar expansion. In fact, the interplanar Ti-Si distance they obtain by image simulations is 1.878 Å. It is significant that this is very close to the ideal and the relaxed distances obtained in models *B* and *C*. As explained by the authors, the images show an apparent ''gap'' between bright spots at both interfaces which might naively be taken as meaning an expansion of the interplanar distance. However, they showed that the best image simulations were obtained when it is assumed that there is a contrast reversal between TiC and SiC. In other words, Ti spots are bright but Si-C pairs (not resolved) correspond to the dark spots. Such a reversal is not an uncommon occurrence.

The next question that comes to mind is why the twinned structure was observed on large flat terraces while the untwinned structure was found only on small (111) facets occurring on step bunched (112) surfaces. Two possibilities may be considered: either the twinned structure has a significantly lower energy, or, the energies for both structures are fairly close and growth kinetics is responsible for the difference in their occurrence. Our present results indicate that the latter is more likely. In fact, to the precision of our calculations we find $\gamma_i^B \approx \gamma_i^C$. The occurrence of the untwinned model for faceted surfaces is easily explained. Kinetic effects due to step edges are well known from the growth of the SiC on off-angle 6*H*-SiC surfaces. The small terrace sizes are found to aid in maintaining the layer stacking of the substrate. The same effect is expected in the present case when steps are present on the TiC surface and terraces are small. It is more difficult to explain why the twinned structure appears to be dominant on flat surfaces. If the energies are as close as our calculations indicate, we would expect to occasionally also find the untwinned arrangement even if the untwinned *C* model would have a slightly higher energy. In favor of this assertion, we note that the SiC grown on top of TiC is found to exhibit numerous microtwins. In opposition to it is in fact that the latter did not seem to originate directly at the interface. We note, however, that to date only one experimental study has been made of the structure of this interface. Significant statistics for the relative frequency of occurrence of twinned versus untwinned interface structures is lacking.

A large energy difference between twinned and untwinned structure as we found between *A* and *B* would make the high energy structure unlikely even in the presence of steps. Thus, the observation of both structures, twinned and untwinned, is, in our opinion, an indication that both structures have nearly equal energies, in agreement with our findings for the small energy difference between *C* and *B*.

B. The Schottky barriers

There are a few factors which make the calculations of a Schottky barrier more difficult than the band offset between two semiconductors[34] particularly those with a small lattice mismatch and the same valencies. For one thing, the difference in the character of the bonding in the two components of the semiconductor/metal system is significant. This can lead to appreciable relaxation at the interface. As noted above, we are including such effects. Secondly, as was pointed out by Das *et al.*,[35] the Schottky barrier height Φ_B^p, although a ground state property and, as such calculable from Kohn-Sham density functional eigenvalues, must in principle include a possible discontinuity in the exchange-correlation potential across the interface. This is not included in the LDA. Unfortunately, no explicit approach is available to compute this discontinuity except for very simplified model systems.[36] From a somewhat different point of view, one may also look at Schottky barrier heights as a difference between one-electron excitation energies, which can be calculated, for example, by means of the *GW* method,[25,37,38] (named after the original notations used in Ref. 25). While the corrections to LDA values found by this approach are typically less than 0.1 eV for interfaces between semiconductors, they are expected to be somewhat larger for those involving a metal. Wenzien *et al.*[39] obtain a value of -0.66 eV for the correction to the valence-band maximum in 3*C*-SiC. Since the correction to LDA is believed to be much smaller in a metal, we take the correction for the Fermi level of TiC to be zero. This would imply that all our LDA values for the Schottky barrier height have to be increased by 0.66 eV. In any case, even if the absolute value of the Schottky barrier height is somewhat uncertain, the LDA calculations should be capable of providing the differences in barrier height for different interface structures. This was demonstrated by Das *et al.*[35] in their calculations for $NiSi_2$/Si. Their calculated Schottky bariers indeed underestimated experimental values by about 0.5 eV but their value for the difference in barriers for twinned and untwinned structures (a situation rather similar to the present one) was in agreement with experiment.

Our method to determine the Schottky barrier closely resembles a procedure often used experimentally. The scheme

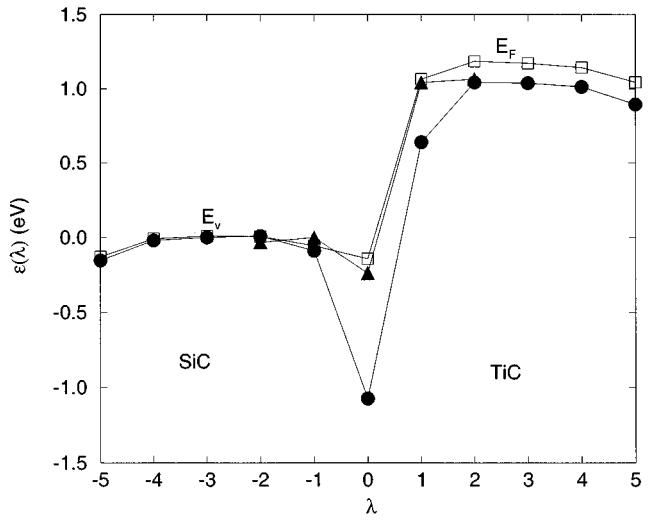

FIG. 5. Schottky barrier determination. The quantity ε defined in the text is shown as function of carbon-layer number λ. It relates to E_v on the SiC side and to E_F on the TiC side. Layer 0 corresponds to the common interface C_i. E_v in the central SiC layer ($\lambda=3$) is chosen as reference so that the values on the right give Φ_B^p directly. The filled circles correspond to the *A*, the open squares to the *B*, and the triangles to the *C* model (for a 3+3 slab).

utilizes the simple fact that in the ''bulk regions'' of the structure the separation of relevant ''valence'' energies (e.g., the Fermi energy of the metal and the valence-band maximum of the semiconductor) from core levels are the same as in the bulk. Thus by using that energy difference along with the position of the core level in the structure $E_c(\lambda)$ at layer number λ, which essentially follows that of the average electrostatic potential in the structure, one obtains the position of the relevant valence energy relative to a common reference energy in the entire structure. The relative position of E_F in the TiC component is thus given by $\varepsilon(\lambda)=E_c(\lambda)+(E_F^{\mathrm{TiC}}-E_{c,0})$, where $E_F^{\mathrm{TiC}}-E_{c,0}$ is the separation of E_F and the core level in bulk TiC. We define ε to be a similar quantity for the SiC component except that it involves the valence-band maximum E_v instead of E_F. Since $\varepsilon(\lambda)$ tracks E_F on the TiC side and E_v on the SiC side, the difference between its two ''asymptotic'' values (those for $\lambda\to+\infty$ and $\lambda\to-\infty$, where $\lambda=0$ at the interface) gives us the Schottky barrier.

In principle, we can use any of the core levels for this procedure, and they need not even be the same on each layer, as long as we use the appropriate $E_F-E_{c,0}$. This was shown in our previous report on the part of this work[24] based on the IDB models. In practice, there are slight variations due to the fact that certain core levels track the electrostatic potential more closely than others and because of slight differences in the bulk and interface computational parameters. In the present case, we use the same core level, the C 1*s*, on both sides of the interface. This seems preferable as it helps to reduce systematic errors. A better approximation of bulklike behavior in the central layers on both sides of the interface is achieved in the larger cells. We thus used the large 6+6 layer slabs for the *A* and *B* structures for this purpose. A 3+3 layer slab was used for *C*. Figure 5 shows the variation of ε with the carbon layer number in the cells for the three models. In this figure we have arbitrarily shifted ε to be zero at layer $\lambda=-3$ on the SiC side. Thus the value of ε on layer $\lambda=3$ on the TiC side immediately gives the Schottky barrier Φ_B^p for *A* and *B*. The layers ±4 and ±5 approach the two surfaces and are thus less bulklike than the layer 3. However, one can clearly see that ε reaches a plateau on either side of the interface within the few layers that comprise our computational unit cell. Thus the curve yields a well-defined Schottky barrier. We obtain Φ_B^p values of 1.0 eV for the *A* structure, 1.2 eV for the *B* structure, and 1.1 eV for the *C* structure. These values are in satisfactory accord with those obtained from the IDB geometry (1.0 eV for *A* and 0.9 eV for *B*) and from an independent estimate using the local densities of states (see below).

The most remarkable thing about these values of the Schottky barrier height is that they are almost the same for all of the structures. The reasons for this will become clear when we examine the electronic structure of the interface in Sec. IV C.

Including the LDA correction mentioned at the beginning of this section, our calculations predict the Schottky barrier to be 1.7 ± 0.1 eV, with the uncertainty taken to be the difference between the two minimum energy structures *C* and *B*. The uncertainty in the LDA corrections is more difficult to evaluate but is certainly larger than that. The above value thus leads to the prediction of a Fermi level position at about 2/3 of the gap measured from the valence-band for 3*C*-SiC ($E_g=2.4$ eV) and about half way in the gap for 6*H*-SiC ($E_g=3.0$ eV).

The Schottky barrier height has to our knowledge not been measured directly. However, it has been determined[10,11] that strongly rectifying behavior occurs for *p*-type SiC while Ohmic behavior could be obtained with n-type SiC. In order to be compatible with our results, we must assume that the Ohmic behavior results from tunneling through the Schottky barrier. The fact that the contact resistance on 3*C*-SiC (Ref. 10) is lower than on 6*H*-SiC (Ref. 11) by a factor of about two could be viewed as being consistent with the fact that our Fermi level is significantly closer to the conduction band edge in 3*C*-SiC than in 6*H*-SiC. However, the difference in the tunneling probability due to the different barrier heights in the two polytypes would be expected to be much larger than a factor of two. The structural quality of the interface undoubtedly plays an important role. In fact, the low values of specific contact resistance are probably primarily due to the better structural quality of the interface along with thin space-charge layers due to heavy *n*-type doping. They do not necessarily reflect a true band lineup of the Fermi level with the conduction band edge. Nevertheless, the above shows that further improvement in the contact resistance would be possible if we could find a means for shifting the Fermi level higher into the gap.

Porter *et al.*[7] reported values for Schottky barrier heights at as-deposited and annealed Ti/6*H*-SiC contacts measured with a variety of techniques: current-voltage (*I-V*), capacitance voltage (*C-V*), and XPS. Formation of an interfacial layer of TiC was observed in these annealed structures, but with an additional formation of Ti silicides further away from the interface with SiC. Because the Fermi levels in the metals (TiC, Ti-silicide, and unreacted Ti) must align, one could thus attempt to interpret the annealed values as corre-

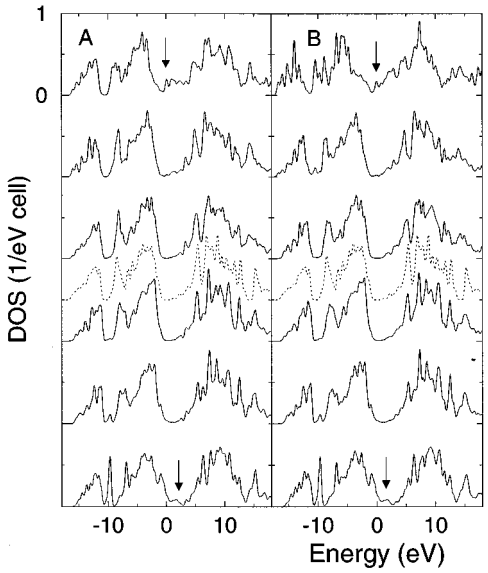

FIG. 6. Densities of states for different layers of SiC in the (6+6) slab geometry for the *A* structure (left graph) and *B* structure (right graph). The upper curve is for SiC at the interface (the C of which are on the mutual carbon layer with TiC), while the curves for the other layers are shifted down. The lowest curve is for SiC at the interface with ''vacuum.'' The energies are relative to the Fermi energy. The dashed curve in the middle shows a bulk SiC DOS for comparison. Arrows indicate interface and surface states.

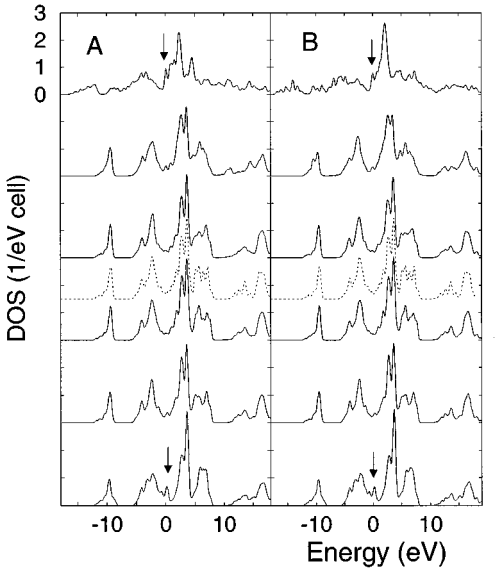

FIG. 7. Densities of states for different layers of TiC in the (6+6) slab geometry for the *A* structure (left graph) and *B* structure (right graph). The upper curve is for TiC at the interface (the *C* of which are on the mutual carbon layer with SiC), while the curves for the other layers are shifted down. The lowest curve is for TiC at the interface with ''vacuum.'' The energies are relative to the Fermi energy. The dashed curve in the middle shows a bulk TiC DOS for comparison. Arrows indicate interface and surface states.

sponding to the SiC/TiC barrier height. However, the interfaces were not homogeneous. The effective barrier height is thus influenced by parts of the interface where Ti silicides or pure Ti is in direct contact with SiC. It may also be influenced by defects occurring at these less well-matched interfaces. This of course makes the interpretation difficult. Nevertheless, their values for the electron SBH, i.e., $\Phi_B^n = E_c - E_F$, are about 0.79–0.88 eV for as-deposited and about 0.86–1.04 eV for annealed. These values are somewhat smaller than the presently calculated values, but, given the uncertainties mentioned, are not too far from our results. Furthermore, since pure Ti/SiC appears to have a smaller SBH than TiC/SiC and influences the effective value for the annealed sample, one could infer that the reported value provides an underestimate of the pure TiC/SiC SBH.

It is also of interest to compare our predicted values with those of the Schottky theory. In that theory, the Schottky barrier height is expected to be simply the difference in work functions. The work function for 6*H*-SiC has been reported to be 4.80 ± 0.05 eV.[40] For the work function of TiC, experimental values between 3.8 and 4.1 have been reported while theoretical calculations gave 4.6 (Refs. 42) and 4.7 eV.[41] The discrepancy between the measured and calculated values was proposed[42] to be due primarily to the existence of carbon vacancies in TiC. In fact, one finds that the work function of TiC_x increases with x. The Schottky theory would thus give a *p*-type Schottky barrier of 0.1–1.0 eV. This is rather different from our value of 1.7 eV. We will show below that the Schottky barrier in this system is strongly influenced by Fermi level pinning at interface states. As such, the Schottky limit is not expected to apply.

C. Electronic structure

In this section we present results for the electronic structure of the interface primarily by inspecting partial densities of states (PDOS). These provide insights into essentially all properties and aspects of the interface, e.g., the interfacial bonding and energetics and the origin of the Schottky barrier height.

Since the PDOS for the IDB models were shown elsewhere,[24] here we present only the results for the slab +slab geometries. These permit a more accurate evaluation of the interface electronic structure features and their decay into the bulk because of the larger number of layers that were employed in these models.

Figures 6 and 7 display the PDOS for the six layers of SiC and the six layers of TiC, respectively, in the *A* and *B* supercells. It is apparent that the shape of PDOS in the second through fifth layers from the interface are almost identical in the two structures. Moreover, they are similar to those for the respective bulk materials, shown in dashed lines, when the latter are appropriately shifted. The shifts in energy required to achieve this ''best alignment'' have uncertainties of at least 0.1 eV. With this alignment, the SiC valence-band maximum is found to occur 0.9 eV below the Fermi level of the slab which coincides with that of bulk TiC. We thus obtain an independent estimate of the Schottky barrier of 0.9 ± 0.1 eV for both models, a result in good agreement with the values obtained above using core levels.

While the PDOS for the second through fifth layers differ very little from each other they differ from that for the sixth layer, which interfaces with ''vacuum'' and which exhibits additional peaks due to surface effects, namely, dangling bonds. These results indicate that the three interfaces in the

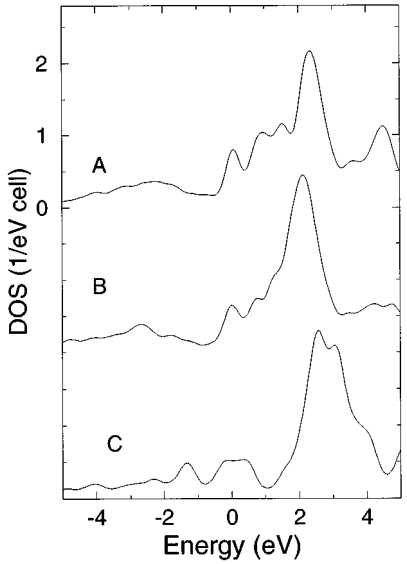

FIG. 8. Densities of states for the Ti layer nearest to the interface for the relaxed *A*, *B*, and *C* structures in the (6+6) slab geometry. The energies are relative to the Fermi energy.

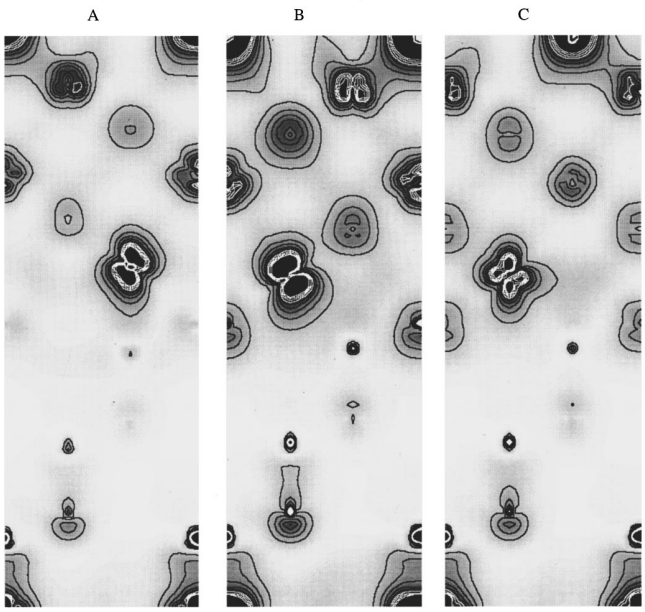

FIG. 9. Partial charge densities of states in a narrow energy window around the Fermi level in models *A*, *B*, and *C* shown as a gray scale and contour lines calculated in 3+3 slab models. The plane passes through the nuclei of all atoms indicated and is the same as the one in Fig. 1.

supercell (one the object of our study, the other two interfaces with the ''vacuum'') have significant effects only on adjacent layers. The PDOS for the SiC adjacent to the interface shows a fairly wide distribution of interface states in the gap, which is indicated by an arrow. These states are commonly referred to as metal induced gap states, or MIG's, and are basically the tails of the TiC states into the SiC.

The PDOS for the Ti layer nearest to the interface is shown in greater detail around the Fermi level Fig. 8. In each of the three structures the Fermi level is located precisely on a DOS peak which does not appear in the bulk. That is, E_F is pinned at an ''interface state.'' The peaks in the *A* and *B* models have very similar amplitudes and widths while that for *C* is broader. The latter appears to be the overlap of the peak corresponding to those in *A* and *B* with the one above it. The Fermi level states are found to have mainly Ti $d\ t_{2g}$ character, with a weak admixture (~ 0.2) of C p functions from analysis of the orbital projected densities of states and partial charge densities shown in Fig. 9. The contributions from Si atoms to these states are negligible. This fact is consistent with the similarity of the interface states in both structures.

The most prominent peak in Fig. 8, which lies at $\sim 2.1-2.3$ eV in the *A* and *B* models and ~ 2.8 eV in *C*, reflects a major Ti peak in bulk TiC. The relative upwards shift of this peak for the *C*-structure results from the fact that interface Ti is not bonded octahedrally to its carbon neighbors.

Figure 9 shows partial charge densities from a region of energy of ± 0.5 eV around the Fermi level. It shows clearly that the largest contribution near the interface is Ti $d\ t_{2g}$ and is very similar in all three models. To identify the atoms in this figure, it is useful to compare it with Fig. 4. The interface occurs roughly in the middle of the figure. The other sizable contributions to the charge density in this energy region appear near the top and bottom of the figure and correspond to surface states. These surfaces states are extraneous to the central concerns of this study; moreover, these surfaces were not relaxed or reconstructed.

Nevertheless, it is clear that the interface states are closely related to corresponding free surface states. Due to the termination of the TiC lattice in Ti with the common C_i layer being more closely bound to SiC, we obtain unbounded Ti d-t_{2g} states which produce a peak at the density of states. At the vacuum end, our model ends with a C layer on the TiC side. Hence the surface states there are somewhat shifted in energy from the ones near the interface. Both are indicated by arrows in Fig. 7. TiC surface states were previously studied by Wimmer *et al.*[41] and Price *et al.*[42] for TiC {001} and by Fujimori *et al.*[43] for both the {111} and {001} surfaces.

Figure 10 displays the DOS for the interfacial carbon layer, the layer which is shared by both the SiC and TiC parts of the structure. As might be expected from the fact that this carbon layer could be considered ''the interface,'' or, at least the layer in the center of the interface, it is the one most sensitive to the details of the structure. Thus greater differences between various spectra might be expected here than in the interface Ti layer (Fig. 8). The most significant overall difference is that the spectra for *B* and *C*, which are generally fairly similar, are shifted downward relative to the spectrum for *A* by roughly 2 eV. This reflects the fact that *B* and *C* have appreciably lower total energies than *A*. Another prominent difference in the three PDOS is the peak at -1.3 eV in the spectrum for *C*.

To pursue the issue further, we show the PDOS for the carbon atoms in the carbon layer adjacent to the interface on the TiC side in Fig. 11. The spectrum for C in bulk TiC is displayed as the dotted curve for comparison purposes. The relevant feature in this set of curves is the reappearance of a peak at -1.3 eV for the C structure. The presence of this

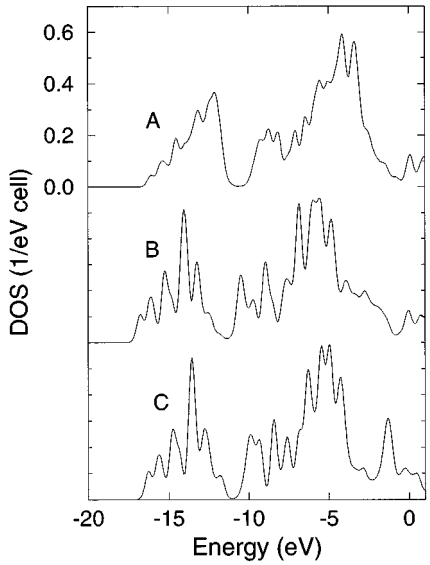

FIG. 10. Densities of states for the interfacial carbon layer for the relaxed *A*, *B*, and *C* structures in the slab geometry. The energies are relative to the Fermi energy.

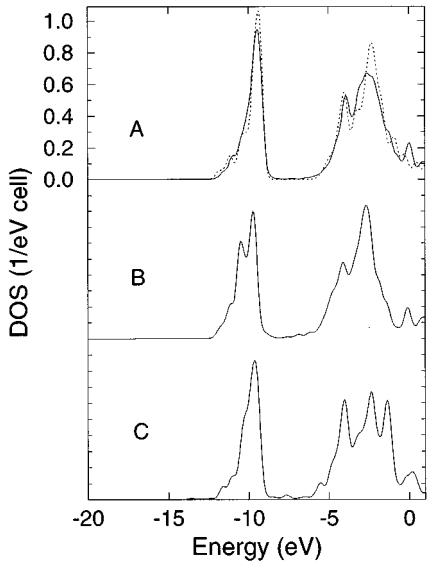

FIG. 11. Densities of states for the carbon layer adjacent to the interface on the TiC side for the relaxed *A*, *B*, and *C* structures in the slab geometry. The superposed dotted line is for bulk TiC. The energies are relative to the Fermi energy.

peak here as well as for the interfacial Ti and C atoms for the c model is again a manifestation of the nonoctahedral bonding of the interfacial Ti to its carbon neighbors.

D. Optical spectra of interface

Since optical properties reflect the electronic structure of a system, it is of interest to see if they could effectively be used to detect the interface states shown here to play an essential role in determining the Schottky barrier height. What makes this an even more attractive possibility than in other interface systems is the fact that SiC is transparent in the visible.

We are concerned here with the optical properties as expressed by the frequency dependent dielectric function associated with direct interband transitions. It is also of interest to see if these properties are sufficiently different for the three structural models that the frequency dependent dielectric function could serve as a tool to distinguish between them.

Because of the presence of the interface there is a unique principal axis of the dielectric function tensor, which is along the normal to the interface. And, because of the threefold symmetry there are two degenerate axes perpendicular to that direction. There are thus two independent components of both the real, $\epsilon_1(\omega)$, and imaginary part, $\epsilon_2(\omega)$, of the complex $\epsilon(\omega)$ tensor. We have calculated the contributions to $\epsilon_2(\omega)$ from the interband transitions including the computation of the dipole matrix elements (see, e.g., Refs. 44,45 for details). The real part, $\epsilon_1(\omega)$, could be obtained from $\epsilon_2(\omega)$ by a Kramers-Kronig transformation if it is needed. Although we used a full-potential method in all other phases of this work, we used the scalar relativistic LMTO method in the ASA (Ref. 46) to obtain the electronic structure used in the calculation of $\epsilon_2(\omega)$. However, the positions of the atoms were taken to be those determined by the FP calculations. The tetrahedron method with 585 $\vec{k}$ points in the irreducible wedge was used for the Brillouin zone integration. The computations were carried out for the three structures. In order to exclude possible contributions from the extraneous surface states which appear from interfaces with the vacuum, we performed all of the dielectric tensor calculations using supercells with the IDB geometry. As was noted in Sec. III, the IDB supercell for the *C* model of the same size as those used for the *A* and *B* models differs from them in that its translation vector lying out of the interface plane is not orthogonal to that plane. That fact, however, does not introduce any fundamental difficulties here. In contrast to the computations of the total energies, here we will not be concerned with quantitative differences between the results for the different structures.

A problem in calculating $\epsilon_2(\omega)$ over even moderately wide energy range for our system arises from the role of corrections to the LDA. In semiconductors, this is frequently referred to as the ''gap problem.'' For the most common polytypes of SiC it was found that a constant shift of about 1 eV of the bands at and above the fundamental band gap is needed to bring the calculated reflectivity into agreement with measured values.[47] This shift is in fairly good accord with that found in recent *GW* calculations.[39] At the present moment, however, we do not have a similar knowledge of the corrections for TiC. We could only anticipate that they would be smaller because TiC is metallic.

These problems are most severe for energies near and above the band gap of SiC. Since we are here primarily concerned with the role of the interface states which are most important at relatively low energies [$<E_g$(SiC)] and are aiming at qualitative effects, we will utilize the LDA bands. We also recall that there are no direct interband transitions in SiC for $\hbar\omega<5.5$ eV and there are only weak contributions from TiC.

Figure 12 shows the interband contributions to $\epsilon_2(\omega)$ for $\hbar\omega<4.0$ eV for the three structures and both polarizations. The major relevant features that can be drawn from Fig. 12 are as follows: (1) though both components of the system are

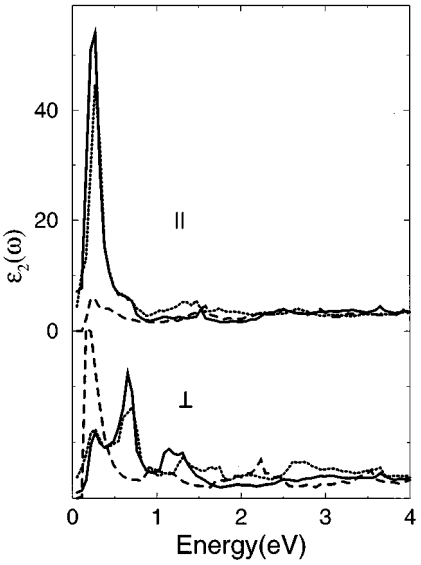

FIG. 12. The imaginary part of dielectric function $\epsilon_2(\omega)$ for light polarized parallel to the interfacial plane (three upper curves) and perpendicular to it (three lower curves). Solid lines are used for the *A* model, dotted for the *B* model, and dashed for the *C* model.

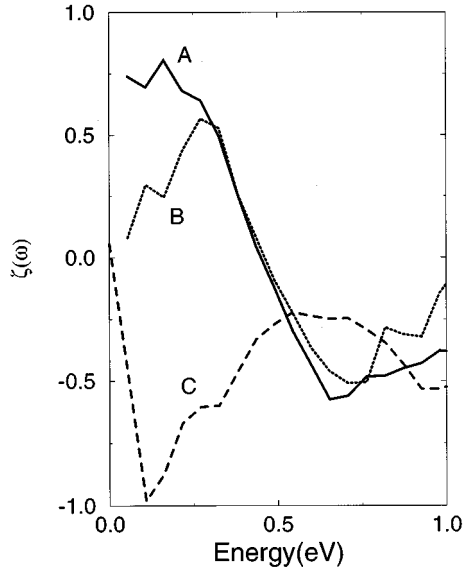

FIG. 13. The polarization ratio function $\zeta(\omega)$ (see text) in the infrared region $\hbar\omega<1$ eV for the three models. Solid line corresponds to the *A* model, dotted to the *B* model, and dashed to the *C* model.

cubic, the components for $\vec{E}\perp\vec{c}$ and $\vec{E}\|\vec{c}$ are quite different — the difference reflecting the presence of the interface; and (2) there are significant differences between the spectra for *A* and *B* on the one hand and *C* on the other. The peaks at low energy arise mainly from interface states around E_F. The strong covalent bonding typical of the carbides strongly admixes the Ti *d* and C *p* states resulting in charge transfer interband transitions.[48] As mentioned earlier, the Si atoms are not strongly involved in the interface states and consequently do not play a significant role in ϵ_2.

To emphasize the contributions from the interface, we have computed the polarization ratio

$$\zeta(\omega)=\frac{\epsilon_{2,\perp}(\omega)-\epsilon_{2,\|}(\omega)}{\epsilon_{2,\perp}(\omega)+\epsilon_{2,\|}(\omega)}, \tag{4}$$

the values of which are restricted to the range -1 to 1. Because contributions from the cubic bulklike regions are polarization independent, they cancel out of ζ. The values of $\zeta(\omega)$ in the infrared region $\hbar\omega<1$ eV for the three models are shown in Fig. 13. The key feature of these results is that while the differences between ζ's for *A* and *B* are relatively small they are huge between those ratios and that for *C*. Our inability to use this optical properties to distinguish between the *A* and *B* structures is in fact not too serious, since the relatively high energy *A* model is, in fact, an unlikely candidate structure. On the other hand, the large differences in the ratios for the likely *B* and *C* structures, particularly for $\hbar\omega<0.5$ eV, suggest a promising means for distinguishing between the two.

The complete dielectric function, of course, also includes the contributions from intraband transitions, namely, the Drude term, which are concentrated at low energies. Since these contributions are proportional to the square of the plasma frequency, ω_p, and that quantity is expected to be less than 10^{-1} of the corresponding value for a good metal, we see that the Drude contributions will be quite weak. Moreover, like the other contributions to $\epsilon_2(\omega)$, those from the bulklike regime will cancel out of ζ. Only those arising from the few layers adjacent to the interface will not completely cancel.

V. SUMMARY

The main results of the paper are as follows. Based on the results of HREM studies and on physical arguments we identified three likely trial structures for the TiC/SiC {111} interface. We calculated and compared their electronic structure and total energies. These models all have a common carbon layer at the interface and a common carbon sublattice shared by the two components. The sublattice is twinned in one of the models. The two low energy structures, labeled *B* and *C*, which are, respectively, twinned and untwinned configurations, are found to have energies which are quite close and are significantly lower than the third structure which is untwinned and denoted *A*. In both of the low energy structures, the Ti atoms are located in the hollow sites in between subsurface Si atoms. The metastable higher energy structure has the Ti directly above the Si in which case there is an unfavorable repulsion between the two. While relaxation accommodates for this Ti-Si bond compression to some extent, it cannot lead to the bond's achieving its equilibrium length without adversely affecting the interfacial Ti-C bonds. This results in a less favorable energetic compromise. The calculations predict an almost perfect interface interplanar distance for both *C* and *B* models. The calculations also predict that the favorable untwinned configuration corresponds to a rigid body translation parallel to the interface so as to bring the Ti into the above-mentioned position. These predictions were shown to be in good agreement with HREM image simulations. The higher energy untwinned *A* structure would have a much larger interplanar spacing and is not consistent

with experimental images. The nearly equal energies of the twinned and untwinned models *B* and *C* indicates that the preferred occurrence of the untwinned configuration on stepped surfaces is related to step-flow growth rather than an energetic difference. The steps ensure the continuation of the cubic stacking. This principle is similar to the stabilization of 6*H*-SiC on stepped 6*H* substrates.[49] The reason for the predominance of the twinned form on large flat areas of (111) surface is not clear given that we find the twinned and untwinned forms to have energies that are so close.

While significant energy differences were found between the *A* model and the *B* and *C* models, we found all three models have almost the same Schottky barriers. This situation is rather different from, for example, $NiSi_2$/Si,[35] and at first rather surprising and interesting. This should, however, not be taken as evidence that Schottky barriers are related to bulk properties only, nor does it support the Schottky theory of Schottky barrier heights, i.e., that they are the differences between work functions. In fact, we find that the Fermi level is strongly pinned by interface states. The explanation for the structure independence is that the states pinning the Fermi level are primarily Ti nonbonding states not participating in the interfacial bond formation. We demonstrated this both using PDOS and plots of interface state charge density. Our analysis of the electronic structure of {111}SiC-TiC interfaces also shows that these states (which appear in the band gap of SiC) are localized within two lattice planes from the interface.

We found the Fermi level to be pinned at about 2/3 of the gap of 3*C*-SiC measured from the valence-band edge when a correction to the LDA for the valence-band maximum of SiC is taken into account. For 6*H*-SiC, the Fermi level position would then be at about midgap if as expected the valence-band maximum to Fermi level lineup is assumed to be the same as in the cubic form. This is in qualitative agreement with the observation of lower specific contact resistance for Ohmic contacts to *n*-type 3*C*-SiC than to 6*H*-SiC. It indicates though that in both cases these are tunneling contacts rather than true band line-up Ohmic contacts.

Finally, we showed that the interface states pinning the Fermi level have a characteristic contribution to the optical response function. Although it lies in the IR and as such may overlap with the rather weak Drude term of bulk TiC, it was shown to posess strong anisotropy with respect to the interface plane which should allow one to distinguish it from bulk contributions. We think this is a promising technique, perhaps along with internal photoemission, to probe these interface states and to experimentally verify the predictions of this theoretical work.

ACKNOWLEDGMENTS

We have enjoyed interesting discussions with F. R. Chien, J. D. Parsons, R. Carpenter, and thank J. S. Bow for sending unpublished micrographs. We also thank M. Sternberg and S. Limpijumnong for assistance with the graphics. Part of the computations were performed at the Ohio Supercomputer Center. This work was supported by Wright-Laboratories under Contract No. F33615-93-C5347.

*Permanent address: P. N. Lebedev Physical Institute, Russian Academy of Sciences, 117924 Moscow, Russian Federation.

[1] *Silicon Carbide and Related Materials 1995*, edited by S. Nakashima, H. Matsunami, S. Yoshida, and H. Harima, IOP Conf. Proc. No. 142 (Institute of Physics and Physical Society, London, 1996).

[2] C. J. Palmstrøm and T. D. Sands, in *Contacts to Semiconductors, Fundamentals and Technology*, edited by L. J. Brillson (Noyes Publications, Park Ridge, 1993), p. 67.

[3] R. Kaplan and V. M. Bermudez, in *Properties of Silicon Carbide*, edited by G. L. Harris, EMIS Datareviews Series Vol. 13 (INSPEC, the Institution of Electrical Engineers, London, 1995).

[4] M. Backhaus-Ricoult, Ber. Bunsenges. Phys. Chem. **93**, 1277 (1989).

[5] J. S. Bow, L. M. Porter, M. J. Kim, W. R. Carpenter, and R. F. Davis, in *Evolution of Surface and Thin Film Microstructure*, edited by H. A. Atwater, E. Chason, M. H. Grabow, and M. G. Lagally, MRS Symposia Proceedings No. 280 (Materials Research Society, Pittsburgh, 1993), p. 571.

[6] J. S. Bow (private communication).

[7] L. M. Porter, R. F. Davis, J. S. Bow, M. J. Kim, R. W. Carpenter, and R. C. Glass, J. Mater. Res. **10**, 668 (1995).

[8] T. Yano, H. Suematsu, and T. Iseki, J. Mater. Sci. **23**, 3362 (1988).

[9] J. J. Bellina, Jr. and M. V. Zeller, in *Novel Refractory Semiconductors*, edited by by D. Emin, T. Aselage, and C. Wood, MRS Symposia Proceedings No. 97 (Materials Research Society, Pittsburgh, 1987), pp. 265 and 283.

[10] J. D. Parsons, G. B. Kruval, and A. K. Chaddha, Appl. Phys. Lett. **65**, 2075 (1994).

[11] A. K. Chaddha, J. D. Parsons, and G. B. Kruval, Appl. Phys. Lett. **66**, 760 (1995).

[12] Q. H. Zhao, J. D. Parsons, H. S. Chen, A. K. Chaddha, J. Wu, G. B. Kruval, and D. Downham, Mater. Res. Bull. **30**, 761 (1995).

[13] G. V. Samsonov and I. M. Vinitskii, *Handbook of Refractory Compounds* (IFI/Plenum, New York, 1980), p. 250.

[14] R. C. Glass, L. M. Spellman, and R. F. Davis, Appl. Phys. Lett. **59**, 2868 (1991).

[15] J. D. Parsons, R. F. Bunshaw, and O. M. Stafsudd, Solid State Technol. **11**, 133 (1985).

[16] J. D. Parsons, in *Novel Refractory Semiconductors* (Ref. 9), p. 271.

[17] J. D. Parsons, R. F. Bunshaw, and O. M. Stafsudd, J. Electrochem. Soc. **140**, 1756 (1993).

[18] F.-R. Chien, S. R. Nutt, and D. Cumming, Philos. Mag. A **68**, 325 (1993).

[19] F.-R. Chien, S. R. Nutt, J. M. Carulli, Jr., N. Buchan, C. P. Beetz, Jr., and W. S. Yoo, J. Mater. Res. **9**, 2086 (1994).

[20] C. J. Palmstrøm, N. Tabatabaie, and S. J. Allen, Jr., Appl. Phys. Lett. **53**, 2608 (1988); C. J. Palmstrøm, S. Mounier, T. G. Finstad, and B. Miceli, *ibid.* **56**, 382 (1990).

[21] S. J. Allen, D. Brehmer, and C. J. Palmstrøm, in *Rare Earth Doped Semiconductors*, edited by G. S. Pomrenke, P. B. Klein, and D. W. Langer, MRS Symposia Proceedings No. 301 (Materials Research Society, Pittsburgh, 1993), p. 307.

[22] D. E. Brehmer, Kai Zhang, Ch. J. Schwarz, S.-P. Chau, S. J. Allen, J. P. Ibbetson, J. P. Zhang, C. J. Palmstrøm, and B. Wilkens, Appl. Phys. Lett. **67**, 1268 (1995).

[23] W. R. L. Lambrecht and B. Segall, Acta Metall. Mater. Suppl. **40**, S17 (1992).

[24] S. N. Rashkeev, W. R. L. Lambrecht, and B. Segall in *Silicon Carbide and Related Materials 1995*, edited by S. Nakashima, H. Matsunami, S. Yoshida, and H. Harima, IOP Conf. Proc. No. 142 (Institute of Physics and Physical Society, Bristol, 1996), p. 309.
[25] L. Hedin and B. I. Lundqvist, J. Phys. C **4**, 2064 (1971).
[26] M. Methfessel, Phys. Rev B **38**, 1537 (1988); M. Methfessel, C. O. Rodriguez, and O. K. Andersen, *ibid.* **40**, 2009 (1989).
[27] R. Ahuja, O. Eriksson, J. M. Wills, and B. Johansson, Phys. Rev. B **53**, 3072 (1996).
[28] M. Methfessel and A. T. Paxton, Phys. Rev. B **40**, 3616 (1989).
[29] N. G. Stoffel, C. J. Palmstrøm, and B. J. Wilkens, Nucl. Instrum. Methods Sect. B **56/57**, 792 (1991).
[30] W. R. L. Lambrecht, C. Amador, and B. Segall, in *Applications of Multiple Scattering Theory to Materials Science*, edited by W. H. Butler, P. H. Dederichs, A. Gonis, and R. L. Weaver, MRS Symposia Proceedings No. 253 (Materials Research Society, Pittsburgh, 1992), p. 381.
[31] N. Chetty and R. M. Martin, Phys. Rev. B **45**, 6089 (1992).
[32] E. Kaxiras, Y. Bar-Yam, J. D. Joannopoulos, and K. C. Pandey, Phys. Rev. B **33**, 4406 (1986).
[33] L. F. Mattheiss and J. C. Hensel, Phys. Rev. B **39**, 7754 (1989).
[34] W. R. L. Lambrecht, B. Segall, and O. K. Andersen, Phys. Rev. B **41**, 2813 (1990); W. R. L. Lambrecht and B. Segall, *ibid.* **41**, 2832 (1990).
[35] G. P. Das, P. Blöchl, O. K. Andersen, N. E. Christensen, and O. Gunnarsson, Phys. Rev. Lett. **63**, 1168 (1989).
[36] O. Gunnarsson and K. Schönhammer, Phys. Rev. Lett. **56**, 1968 (1986); O. Gunnarsson (private communication).
[37] M. S. Hybertsen and S. G. Louie, Phys. Rev. B **34**, 5390 (1986).
[38] R. W. Godby, M. Schlüter, and L. J. Sham, Phys. Rev. B **37**, 10 159 (1988).
[39] B. Wenzien, P. Käckell, F. Bechstedt, and G. Cappellini, Phys. Rev. B **52**, 10 897 (1995).
[40] J. Pelletier, D. Gervais, and C. Pomot, J. Appl. Phys. **55**, 994 (1984).
[41] E. Wimmer, A. Neckel, and A. J. Freeman, Phys. Rev. B **31**, 2370 (1985).
[42] D. L. Price, B. R. Cooper, and J. M. Wills, Phys. Rev. B **46**, 11 368 (1992); **48**, 15 311 (1993).
[43] A. Fujimori, F. Minami, and N. Tsuda, Surf. Sci. **121**, 199 (1982).
[44] M. Alouani, L. Brey, and N. E. Christensen, Phys. Rev. B **37**, 1167 (1988), and references therein.
[45] E. G. Maksimov, I. I. Mazin, S. N. Rashkeev, and Yu. A. Uspenski, J. Phys. F **18**, 833 (1988), and references therein.
[46] O. K. Andersen, Phys. Rev. B **12**, 3060 (1975); O. K. Andersen, O. Jepsen, and M. Sob, in *Electronic Band Structure and its Applications*, edited by M. Yussouf (Springer, Heidelberg, 1987).
[47] W. R. L. Lambrecht, B. Segall, W. Suttrop, M. Yoganathan, R. P. Devaty, W. J. Choyke, J. A. Edmond, J. A. Powell, and M. Alouani, Appl. Phys. Lett. **63**, 2747 (1993); Phys. Rev. B **50**, 10 722 (1994).
[48] A. G. Nargizyan and S. N. Rashkeev, Z. Phys. B **82**, 217 (1991).
[49] H. Matsunami and T. Kimoto, in *Diamond, SiC and Nitride Wide Bandgap Semiconductors*, edited by C. H. Carter, Jr., G. Gildenblat, S. Nakamura, and R. J. Nemanich, MRS Symposia Proceedings No. 339 (Materials Research Society, Pittsburgh, 1994), p. 369.